NANO LETTERS

pubs.acs.org/NanoLett Letter

Chemochromism and Tunable Acoustic Phonons in Intercalated MoO_3: Ag-, Bi-, In-, Mo-, Os-, Pd-, Pt-, Rh-, Ru-, Sb-, and W-MoO_3

Bryan W. Reed, Ethan Chen, and Kristie J. Koski*

Cite This: *Nano Lett.* 2024, 24, 11954−11959 Read Online

ACCESS | Metrics & More | Article Recommendations | Supporting Information

ABSTRACT: Intercalation of several elements (Ag, Bi, In, Mo, Os, Pd, Pt, Rh, Ru, Sb, and W) is used to chemically alter a wide range of properties of two-dimensional layered α-MoO_3. Intercalation modifies acoustic phonons and elastic constants, as measured with Brillouin scattering. Intercalation alters electronic bandgaps, color, structure, Raman shifts, and electron binding energies. Optical chemochromism is demonstrated with intercalants changing the color of MoO_3 from transparent to brilliant blue (In, Mo, Os, and Ru) and orange (Ag). Correlations are investigated among material properties. There is evidence that in-plane longitudinal stiffness c_{11} correlates with changes in the bandgap, while various Raman modes appear to be connected to a variety of properties, including shear modulus c_{55}, Mo binding energies, lattice constants, and the preferred crystal structure of the intercalant. The results indicate a surprising degree of complexity, suggesting competition among multiple distinct mechanisms and interactions involving specific intercalant species.

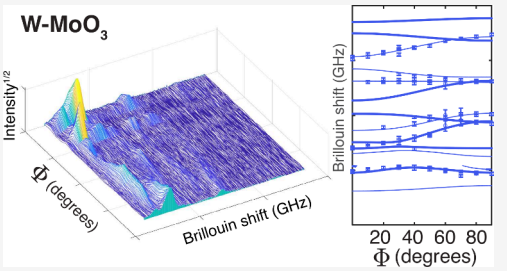

KEYWORDS: *MoO_3, Brillouin scattering, acoustic phonons, intercalation, elasticity*

Downloaded via UNIV OF CALIFORNIA DAVIS on November 26, 2024 at 19:09:26 (UTC).
See https://pubs.acs.org/sharingguidelines for options on how to legitimately share published articles.

α-MoO_3 is one of the most diversely applied intercalation oxides. It exhibits a flexible array of characteristics that change upon intercalation, including the ability to change color,[1,2] electrochromism,[3,4] chemical switching of polaritons,[5] surface-enhanced Raman effects,[6] intercalation tunable bandgaps,[2,7] antibiotic resistance,[8] and nonlinear optical absorption.[9] Recently, it was shown that the optical and elastic properties of MoO_3 can be altered by intercalating as little as ≤1 atm % Cu, Co, Sn, Au, Fe, Cr, Ge, Mn, and Ni.[1,2] Here, we intercalate Ag, Bi, In, Mo, Os, Pd, Pt, Rh, Ru, Sb, and W into α-MoO_3 to explore the full chemical tunability of the mechanical and optical properties, bringing the total number of intercalant species to 20 when the previous studies are included.[1,2] Intercalants can change the color of MoO_3 from transparent to orange and dark blue. Intercalation can also reduce the electronic bandgap of MoO_3 by >1 eV while modifying the elastic stiffness coefficients by up to tens of gigapascals. The changes in stiffness coefficients are manifested in changes in the acoustic phonon propagation speeds as determined through Brillouin scattering of generalized Lamb modes confined within ∼200 nm thick nanoribbons.

We performed correlation analysis on this library of 20 different intercalants to explore possible underlying patterns or principles that govern how elastic and other properties are altered with intercalation. In addition to the stiffnesses as determined through Brillouin scattering, we also considered results from Raman spectroscopy, X-ray photoelectron spectroscopy (XPS), ultraviolet photoelectron spectroscopy (UPS), X-ray diffraction (XRD), and ultraviolet−visible (UV−vis) spectroscopy along with literature values for the properties of the intercalant atoms. In searching for correlations among these many variables, we sought to determine whether relatively simple intuitive descriptions might capture much of the variability.

What we found were complexity and richness of behavior. There are some patterns that may be interpreted in terms of concepts, such as intercalant−host charge transfer. There are numerous strong apparent correlations, most notably involving certain Raman shifts, the lattice constant related to the expansion of the van der Waals gap, stiffness tensor elements governing in-plane deformation (c_{11} and c_{55}), the electronic bandgap of the intercalated material, and the preferred crystal structure of the intercalating elements.

Most properties of the intercalant show no strong correlation with changes in stiffness, but we find a correlation of stiffnesses c_{11} and c_{23} with the electronic bandgap. We also find a correlation of in-plane shear modulus c_{55} with the Raman shifts, as well as the preferred crystal structure of the intercalant. We find several other likely correlations among the Raman shifts, the *b* lattice constant, and the Mo 3d binding energy.

Received: July 12, 2024
Revised: September 10, 2024
Accepted: September 11, 2024
Published: September 13, 2024

ACS Publications © 2024 American Chemical Society

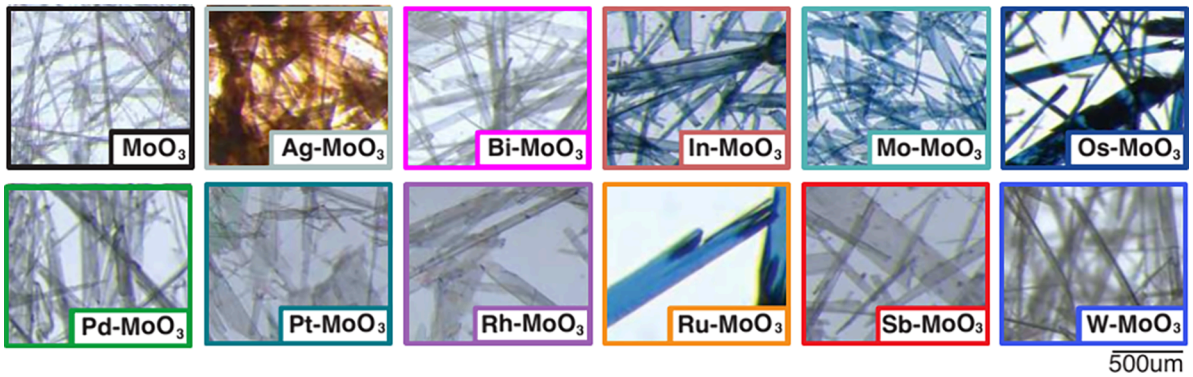

Figure 1. Optical images of Ag-, Bi-, In-, Mo-, Os-, Pd-, Pt-, Rh-, Ru-, Sb-, and W-intercalated MoO_3 showing a diverse change in color with intercalation. Color changes range from transparent to orange, gray, and light blue to dark blue.

α-MoO_3 has a layered orthorhombic crystal structure (space group *Pbnm*). Synthesis of the host and intercalation were performed using established procedures.[1,10,11] Details of growth and intercalation can be found in the Supporting Information. Intercalation concentrations were kept below 5 atm % so as not to disrupt the crystal symmetry and simplify analysis of the Brillouin scattering data. Changes in the material properties are significant at even low intercalant concentrations. Scanning electron microscope energy X-ray dispersive spectroscopy (SEM-EDX) and XPS were used to determine intercalant concentrations. Further details and spectra can be found in Figure S1.

MoO_3 (~200 nm thick) is transparent (Figure 1) but is chemochromic upon intercalation.[1,2] Here, intercalation leads to a vast array of color changes in MoO_3. Intercalation with Bi, Pd, Pt, Rh, Sb, and W shows almost no change in color, though it possibly induces a gray color in the case of Pd. Intercalation with In, Mo, Os, or Ru shows a striking color change to dark blue. When intercalated with Ag, MoO_3 shows an orange color possibly related to silver's plasmonic properties similar to the orange-brown color seen in other Ag nanoparticle oxide thin film systems.[14]

UV−vis absorption (Figure 2a) was collected via transmission. Tauc plot analysis was used to determine the electronic bandgap (Figure S2). In the region from 550 to 800 nm, a strong absorption peak is seen for Ru-, Os-, and In-intercalated MoO_3, consistent with the striking dark blue color seen in those ribbons (Figure 2a). Similar strong absorption was seen for Cr, Ge, and Mn intercalants.[2] Figure 2b shows the electronic bandgaps determined from Tauc plot analysis. Intercalation with Bi slightly increases the effective bandgap, while all other intercalants decrease the bandgap (Figure 2b). Pd and Ni decrease the bandgap substantially to ~2.4 eV.

XRD (Figure 2c) of MoO_3 gives one set of lattice reflections corresponding to stacking direction (0*k*0) and another weak reflection corresponding to (110). Rietveld refinement was performed using MAUD[13] to determine the *b* lattice constant, which is in the stacking direction (Figure 2d). The *b* lattice constant decreases for Bi, in an interesting correlation with the increase in the electronic bandgap of that element, while all other intercalants show an increase. Os and Ru show a doublet in their XRD spectra similar to intercalation of Hf in MoO_3.[12] This was also found for deintercalation of MoO_3 using H_2O_2, where some of the guest is left in the host leading to separate regions of expanded and contracted MoO_3.[15] The domain

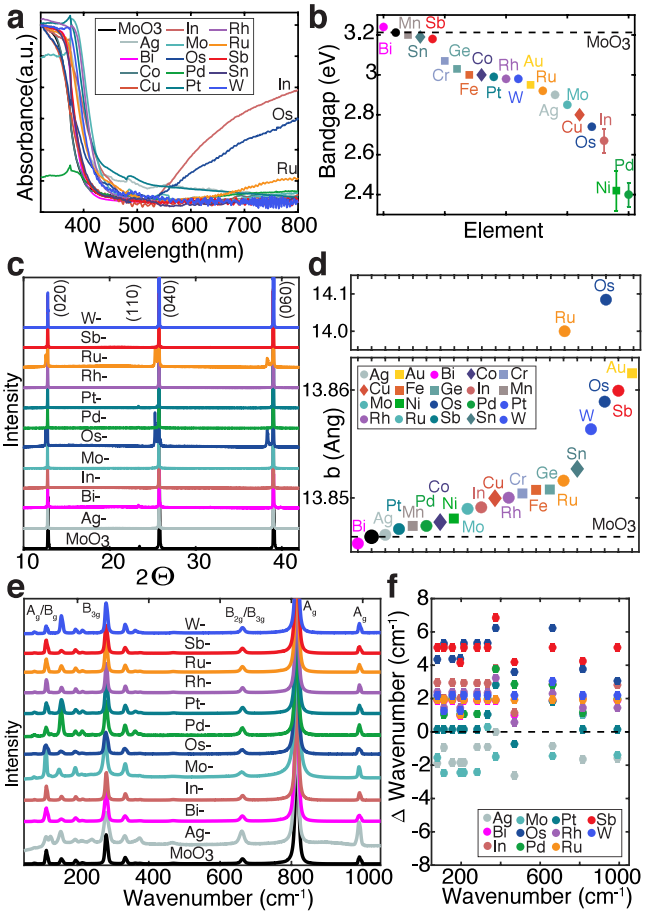

Figure 2. (a) UV−vis spectra of intercalated MoO_3 showing a shift in the absorption edge and absorption above 600 nm for Ru, Os, and In intercalation. (b) Effective electronic bandgap with intercalation. Filled diamonds (♦) are from ref 1, and filled squares (■) are from ref 2. (c) XRD of intercalated MoO_3 (d) shows expansion of the host and doublets for Os and Ru. (e) Raman spectra of intercalated MoO_3 shows both (f) optical phonon stiffening and softening from pristine MoO_3. Pristine MoO_3 XRD and Raman from ref 1.

nature of intercalation into a host may account for this separation.[16,17]

Raman scattering (Figure 2e) of intercalated MoO_3 shows the expected modes.[18] Ag-intercalated MoO_3 shows two new Raman peaks not seen in pure MoO_3 at 123.9 and 241.1 cm^{-1}, which correspond to B_{2g} and B_{1uT} modes,[18] respectively. Pd

https://doi.org/10.1021/acs.nanolett.4c03198
Nano Lett. 2024, 24, 11954−11959

intercalation shows a new mode at 125.8 cm^{-1} corresponding to a B_{2g} mode.[18] No other intercalants show new Raman modes. Raman scattering (Figure 2f) shows both stiffening (Bi, In, Os, Pd, Pt, Rh, Ru, Sb, and W) and softening (Ag, Mo, and Pt) of pristine MoO_3, which is given as a dotted line in Figure 2f. Raman shifts are known to be complex upon intercalation.[19] The guest intercalant can act as a donor or acceptor altering bond strengths and the Raman shift while also changing the local polarizability in a competing manner.[19] Structural changes also affect the Raman shift.[19]

XPS was used to confirm the intercalant concentration and identify charge transfer between the MoO_3 and intercalant. In surprising contrast to previous investigations,[2] XPS of these intercalants (Figure 3a,b) shows a much more diverse behavior

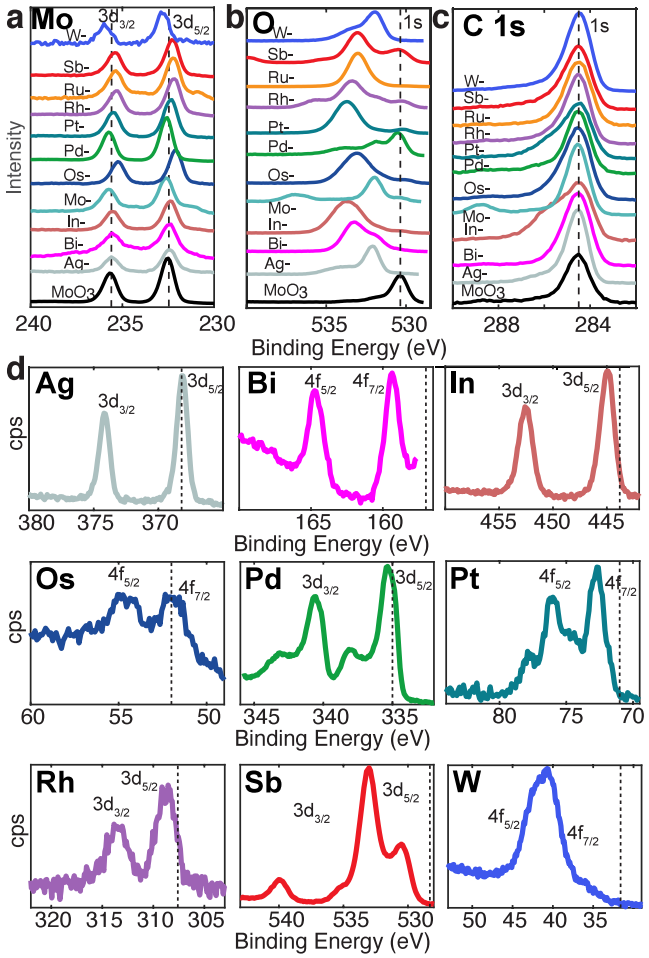

Figure 3. XPS spectra of intercalated MoO_3 show changes in the binding energy of the (a) Mo 3d and (b) O 1s. (c) Adventitious C 1s is used as a calibrant. Pristine MoO_3 (ref 2) shown for comparison. (d) Individual spectra of Ag-, Bi-, In-, Os-, Pd-, Pt-, Ru-, Sb-, and W-intercalated MoO_3 show the metal is in the host. A dotted line is drawn to indicate the peak location[20] for the zero-valent species.

of host−intercalant charge transfer. Not all intercalants lead to a reduction of the Mo, in contrast to the case for MoO_3 bronzes, as seen in both the shift and lack of additional peaks in the XPS spectra.[21] Adventitious C 1s (284.5 eV) is used for calibration (Figure 3c).[20] Generally in XPS, an increase in binding energy means a decrease in electron density (electrons are withdrawn), while a decrease means the reverse. Mo 3d XPS peaks (Figure 3a) with some intercalants show no shift and thus no electron transfer (Ag, Bi, and In). Other intercalants show a decrease in the Mo 3d peaks (Os, Pt, Rh, Ru, and Sb), suggesting that electrons are withdrawn from the Mo, while yet others show an increase in the Mo 3d binding energies (Mo, Pd, and W), suggesting that for those intercalants guest electrons are donated to the host. The O 1s XPS spectra (Figure 3a) show an increase in binding energy for all intercalants except Pd and Sb, suggesting that electrons are withdrawn from the oxygen for nearly all of the intercalated materials.

Figure 3d shows the XPS spectra of the intercalated species. It is not possible to resolve the Ru peaks (280 keV) or the Mo intercalant peaks, as they overlap with adventitious C 1s and the host MoO_3, respectively. Guest species are detected in all other samples. Black dashed lines are drawn to indicate the published[20] peak locations for the zero-valent species.

Brillouin scattering measurements and analysis were performed using published methods[1,2] using an equal-angle (90°) scattering geometry (Figure 4a). The sample was rotated azimuthally around the *b*-axis (normal to the nanoribbon surface), thereby probing phonon dispersion as a function of azimuthal angle Φ. Φ is defined so that phonon propagation parallel to the *a*-axis is probed at Φ = 0°, while propagation parallel to the *c*-axis is probed at Φ = 90°. Measurements were performed through a full 180° rotation for each sample. This allows us to verify the expected symmetry such that Φ and 180° − Φ produce the same results. This was true to within small discrepancies for most samples, allowing us to establish an error floor of ±~0.25 GHz in Brillouin peak positions as in previous work.[1,2]

This repeatability test sometimes failed for the Mo and Ru intercalants, often accompanied by a visible change in the color of the sample over the hours required for a full azimuthal scan. Intercalated Mo-MoO_3 and Ru-MoO_3 may be chemically less stable, or the Ru and Mo species may be more mobile in the host; this may introduce unknown systematic errors into the stiffness tensors in these cases.

Waterfall plots of the raw data can be found in Figure S5. We identified the peaks in each spectrum, which as a function of angle Φ revealed angular dispersion relations of various acoustic modes (Figure 4b). We identify these as Love modes (L), antisymmetric Lamb modes (AS_L), and symmetric Lamb modes (S_L) as illustrated in Figure 4c and extract the stiffness tensor through curve fitting.[1,2] This yields estimates for all nine independent elastic moduli along with sample thickness *d*. Errors in the fit parameters are determined from χ^2 analysis ultimately grounded in the counting statistics of the detector.[1,2]

Table 1 lists the thicknesses and elastic stiffnesses. Intercalation has strong effects on the elastic moduli, shifting values by tens of gigapascals in complex patterns particular to each intercalant. Similar previous measurements[1,2] were performed on pure MoO_3 as well as MoO_3 intercalated with Co, Cu, Sn, Fe, Ge, Ni, Mn, Cr, and Au, in which general trends of the effects of intercalants on specific stiffness coefficients were observed, with some outliers. With the addition of more data, including 11 new intercalants in this work, we find the story becomes much more complex, with many of the intercalants acting as unique outliers, each altering the stiffness tensor in its own way. The trends are described in detail in the Supporting Information.

We find an apparent correlation between *d* and some of the stiffness tensor elements, especially not only c_{22} but also c_{12}, c_{44}, and c_{66}. Given the thickness-dependent nature of intercalant

https://doi.org/10.1021/acs.nanolett.4c03198
Nano Lett. 2024, 24, 11954−11959

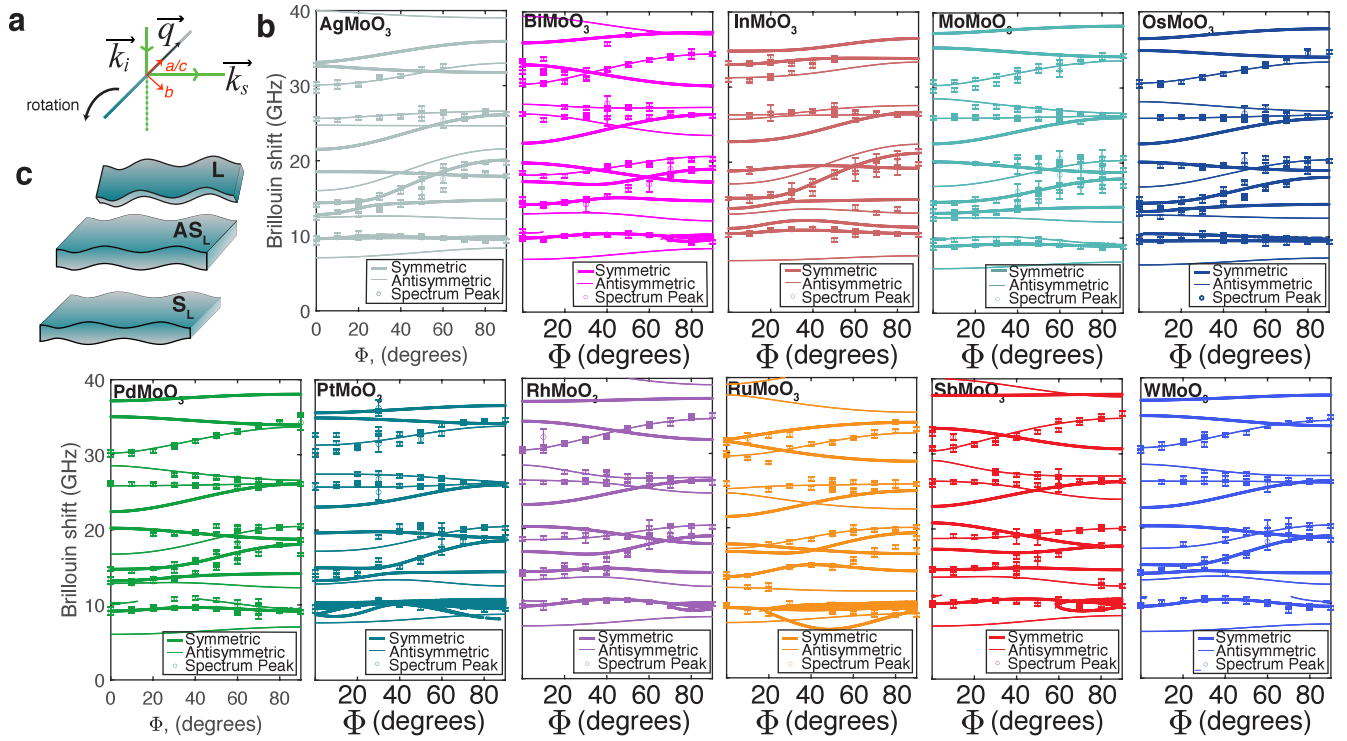

Figure 4. (a) Equal-angle (90°) Brillouin scattering geometry used for measurements. The sample is rotated azimuthally around the normal axis (*b*). k_i and k_s are the input and output scattering wavevectors, respectively. q is the phonon wavevector. (b) Illustrative representations of Love waves (L), antisymmetric Lamb (AS_L) modes, and symmetric Lamb (S_L) phonon modes. (c) Brillouin scattering spectra of all intercalated materials with curve fits.

Table 1. Thicknesses, d (nm), and Elastic Stiffnesses, c_{ij} (GPa), of Intercalated MoO_3 Determined from Brillouin Scattering[a]

	d	c_{11}	c_{22}	c_{33}	c_{12}	c_{13}	c_{23}	c_{44}	c_{55}	c_{66}
MoO_3[1]	186.1(2)	156(2)	128.7(8)	241(2)	−13(2)	31(2)	35(2)	51.6(3)	60(1)	38.0(2)
Ag-MoO_3	234.3(6)	118(1)	195(1)	267(1)	−20(1)	38(1)	10(1)	64.6(4)	61.3(4)	58.9(4)
Bi-MoO_3	225(3)	185(3)	195(6)	239(3)	−38(3)	50(3)	20(4)	70(1)	65(1)	48(1)
In-MoO_3	199(4)	141(4)	153(5)	297(4)	−17(3)	30(4)	17(7)	46(3)	73(1)	48(3)
Mo-MoO_3	176(3)	136(2)	106(2)	212(2)	−14.2(9)	53(2)	−7(2)	48(1)	52.6(4)	39.6(6)
Os-MoO_3	190(2)	130(3)	127(2)	213(2)	−12(2)	43(3)	−5(3)	52(1)	59(1)	45(1)
Pd-MoO_3	183(3)	133(3)	115(2)	216(2)	−16(1)	41(2)	−5(2)	50.8(4)	55.8(9)	41.9(6)
Pt-MoO_3	236.7(4)	133.3(2)	197.8(2)	228(2)	−24.1(2)	24(2)	14(3)	77.4(5)	60.0(5)	70.8(5)
Rh-MoO_3	214(2)	183(4)	166(4)	238(4)	−25(3)	44(3)	29(4)	68.2(7)	62(1)	49(1)
Ru-MoO_3	250(1)	165(1)	228(1)	245(1)	−50(1)	68(1)	39(1)	68(1)	58(1)	55(1)
Sb-MoO_3	221(2)	193(3)	183(2)	208(2)	−25(2)	42(2)	13(3)	75.9(8)	67(1)	48.0(7)
W-MoO_3	185(4)	147(3)	125(5)	235(5)	−11(2)	28(3)	25(4)	51(2)	61(1)	42(1)

[a]Data for unintercalated MoO_3 are from ref 1. Values in parentheses are errors in the last digit, as determined by nonlinear curve fitting analysis.

staging, it is plausible that these moduli are genuinely functions of nanoribbon thickness for the intercalated material. However, it is also plausible that some of this correlation reflects an artificial coupling of the d fit parameter to some of the stiffness coefficients in the nonlinear curve fit. While our method of estimating the errors in the fit parameters (see ref 2) is designed to avoid such issues, it is still possible that the error bars reported in Table 1 may be underestimates for these four stiffness coefficients as well as d. This issue does not affect the other five coefficients. See the Supporting Information for more details.

Combining results from our study and previous studies,[1,2] we have extensively characterized the physical properties of 21 different variants of MoO_3. The data include d and c_{ij} from Brillouin measurements; the stiffness tensor, bulk modulus, Young's moduli, and Poisson's ratios; the b lattice constant; the bandgaps; 12 distinct Raman peaks; and binding energies for Mo and O. To this we added literature properties of the pure element intercalant itself: electronegativity, work function, covalent radius, and native crystal structure.[10] We searched this entire data set for pairwise correlations to identify any evidence of regularities and likely mechanisms explaining one set of properties in terms of another (Figures S6–S12). Figure 5 shows the strongest correlations that we found.

All of the Raman modes strongly correlate to each other. We find that each individual Raman mode seems to have particularly strong correlations with several other properties. For example, we find an anticorrelation of the Raman shift with the increase in Mo binding energy, especially for the Raman mode near 114 cm^{-1} (Figure 5a). A higher binding energy is

https://doi.org/10.1021/acs.nanolett.4c03198
Nano Lett. 2024, 24, 11954−11959

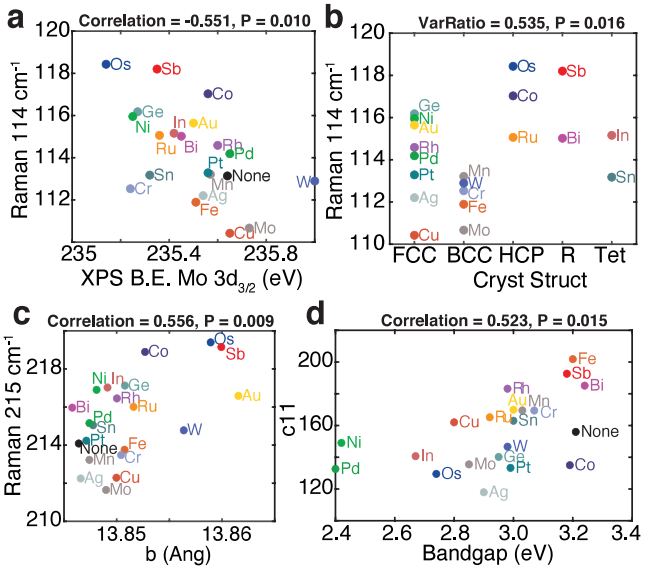

Figure 5. Strongest correlations. (a) Anticorrelation of the binding energy shift of the XPS Mo $3d_{3/2}$ spectra vs Raman shift. (b) Correlation of the preferred crystal structure of the unintercalated element vs Raman shift. (c) Lattice constant, b, vs Raman shift. (d) Bandgap vs c_{11}.

correlated with softer Raman modes, which is measured through the charge transfer from the guest to host in XPS.

We also find that the Raman shifts correlate with both the preferred bulk crystal structure of the intercalant and the expansion of the host (Figure 5b,c). The intercalants with a hexagonal close-packed (HCP) or rhombohedral (R) native crystal structure uniformly had Raman shifts that were larger than those with body-centered cubic (BCC) structures. A correlation of intercalated material properties with the native crystal structure of the intercalating element is not unprecedented. Koski et al.[10] found that, in Bi_2Se_3, the unit cell volume of change correlated with the bulk crystal structure of the intercalant. We suspect that the preferred atomic arrangements (i.e., bond angles and preferred local symmetry) of the elements in their native crystal structure are also in part manifested in their preferred locations and bonding patterns within the van der Waals gap of the intercalated structure. In our results, while the b lattice constant and the intercalant's native crystal structure both correlate with the Raman shifts, they do not significantly correlate with each other. We also found weak evidence that b correlates positively with the electronegativity of the intercalant (Figure S12).

We also observed some likely correlations involving the stiffness tensor. The measured bandgap of the intercalated material appears to correlate positively with c_{11} and c_{23} (Figure 5d and Figure S7). The Raman mode near 155 cm^{-1} appears to correlate with in-plane shear modulus c_{55} (Figure S8). This has been identified as A_g bending mode $\delta(O_xMo_2)_n$.[18,22] Both Raman modes and the stiffness tensor give us information about the stiffness of bonds in the context of the crystal lattice. However, they do so on very different length scales. If the information about the stiffness of specific groups of bonds as revealed in Raman spectroscopy is somehow encoded in the stiffness tensor elements, then a simple correlation analysis does not appear to be sufficient to extract it, with the possible exception of the apparent correlation between c_{55} and the Raman mode near 155 cm^{-1}.

Intercalant properties such as atomic size, electronegativity, work function, etc., do not strongly correlate with the change in the stiffness tensor. For the most part, the combined data set tells a story of complexity. The ability of the various intercalants to modulate the material properties is multidimensional, resisting efforts to reduce it to a short list of persistent patterns, simple recipes, or easily understood mechanisms such as a uniform charge transfer between the host and intercalant, an overall shift in polarizability, etc. Rather, the complexity we observe suggests that there are multiple competing mechanisms, some of which may be particular to certain excitation modes or certain intercalant species.

In summary, this study uses the methodology of previous studies[1,2] to generate a substantial database quantitatively by recording the effects of many different intercalants on the optical, electronic, structural, mechanical, and bonding properties of MoO_3. Combined with the previous studies, this study more than doubles the number of intercalants, bringing the total to 20. We show how various intercalants can alter the elastic stiffness coefficients of MoO_3 by up to tens of gigapascals, significantly decreasing the bandgap and also changing the color, sometimes quite strongly. Unique effects specific to each intercalant are seen in the physical property changes of MoO_3 with intercalation.

By more than doubling the number of material states in the data set, we found a range of complexity of behavior that was previously hidden. What the data tell us is that there is no simple systematic story that can account for all of the variability. Instead, there are likely many competing phenomena. Each intercalant alters the material in its own peculiar way. While this may be challenging from a basic science perspective, from an application perspective, it means the space of possible material alterations is much larger than we had first imagined. The bandgap, color, optical properties, anisotropic stiffness, and other properties can potentially all be modulated independently of one another based on the choice of intercalants.

■ ASSOCIATED CONTENT

Supporting Information

The Supporting Information is available free of charge at https://pubs.acs.org/doi/10.1021/acs.nanolett.4c03198.

Experimental details, including materials, methods, synthesis and characterization, additional SEM-EDX characterization of MoO_3, UV−vis Tauc plot analysis, UPS results, rotational Brillouin scattering spectra for all intercalants, table of bulk moduli and Young's moduli, table of Poisson ratios, σ_{ij}, p values and linear correlation coefficients of experimental values and stiffnesses, and plots of relevant correlations for all intercalants (PDF)

■ AUTHOR INFORMATION

Corresponding Author

Kristie J. Koski − *Department of Chemistry, University of California Davis, Davis, California 95616, United States;* orcid.org/0000-0002-5250-2593; Email: koski@ucdavis.edu

Authors

Bryan W. Reed − *Integrated Dynamic Electron Solutions, Pleasanton, California 94588, United States;* orcid.org/0000-0003-3629-2853

https://doi.org/10.1021/acs.nanolett.4c03198
Nano Lett. 2024, 24, 11954−11959

Ethan Chen − *Department of Chemistry, University of California Davis, Davis, California 95616, United States;* orcid.org/0009-0009-8642-1642

Complete contact information is available at: https://pubs.acs.org/10.1021/acs.nanolett.4c03198

Notes

The authors declare no competing financial interest.

■ ACKNOWLEDGMENTS

The authors acknowledge funding from the National Science Foundation (DMR-2202472). E.C. acknowledges funding from the AMPAC Fine Chemicals Undergraduate Research Fellowship.

■ REFERENCES

(1) Reed, B. W.; Williams, D. R.; Moser, B. P.; Koski, K. J. Chemically tuning quantized acoustic phonons in 2D layered MoO_3 nanoribbons. *Nano Lett.* **2019**, *19*, 4406−4412.

(2) Reed, B. W.; Chen, E.; Koski, K. J. Tunable Chemochromism and Elastic Properties in Intercalated MoO_3: Au-, Cr-, Fe-, Ge-, Mn-, and Ni-MoO_3. *ACS Nano* **2024**, *18* (20), 12845−12852.

(3) Arnoldussen, T. C. Electrochromism and photochromism in MoO_3 films. *J. Electrochem. Soc.* **1976**, *123*, 527−531.

(4) Müller-Warmuth, W.; Schöllhorn, R. *Progress in intercalation research*; Springer Science & Business Media, 2012; Vol. *17*.

(5) Wu, Y.; Ou, Q.; Yin, Y.; Li, Y.; Ma, W.; Yu, W.; Liu, G.; Cui, X.; Bao, X.; Duan, J.; et al. Chemical switching of low-loss phonon polaritons in α-MoO_3 by hydrogen intercalation. *Nat. Commun.* **2020**, *11*, 2646.

(6) Wang, H.; An, G.; Xu, S.; Xu, Q. Fe and Cu Intercalations Enhance SERS of MoO_3 through Different Mechanistic Pathways. *Chem. - Eur. J.* **2024**, *30*, e202303391.

(7) Lin, J.; Chen, H.; Ma, D.; Gong, Y.; Li, Z.; Li, D.; Song, Y.; Zhang, F.; Li, J.; Wang, H.; et al. Band structure tuning of α-MoO_3 by tin intercalation for ultrafast photonic applications. *Nanoscale* **2020**, *12*, 23140−23149.

(8) Liu, H.; Zuo, Y.; Lv, S.; Liu, X.; Zhang, J.; Zhao, C.; Xu, X.; Xu, Y.; Wang, X. Ultralow Loading Copper-Intercalated MoO_3 Nanobelts with High Activity against Antibiotic-Resistant Bacteria. *ACS Appl. Mater. Interfaces.* **2024**, *16*, 17182−17192.

(9) Hou, R.; Li, H.; Zhang, C.; Huang, Z.; Humphrey, M. G. Effect of ion intercalation and electrochemisorption on nonlinear optical absorption of MoO_3: A comparative study of six different ions. *J. Nonlinear Opt. Phys. Mater.* **2024**, *33*, 2340006.

(10) Koski, K. J.; Wessells, C. D.; Reed, B. W.; Cha, J. J.; Kong, D.; Cui, Y. Chemical intercalation of zerovalent metals into 2D layered Bi_2Se_3 nanoribbons. *J. Am. Chem. Soc.* **2012**, *134*, 13773−13779.

(11) Wang, M.; Williams, D.; Lahti, G.; Teshima, S.; Dominguez Aguilar, D.; Perry, R.; Koski, K. J. Chemical intercalation of heavy metal, semimetal, and semiconductor atoms into 2D layered chalcogenides. *2D Mater.* **2018**, *5*, 045005.

(12) Huynh, V.; Rivera, K. R.; Teoh, T.; Chen, E.; Ura, J.; Koski, K. J. Hafnium, Titanium, and Zirconium Intercalation in 2D Layered Nanomaterials. *ACS Nanosci. Au* **2023**, *3*, 475−481.

(13) Lutterotti, L.; Matthies, S.; Wenk, H. MAUD: a friendly Java program for material analysis using diffraction. *IUCr: Newsletter of the CPD* **1999**, *21*, 14−15.

(14) Kafizas, A.; Dunnill, C.-W.; Parkin, I.-P The relationship between photocatalytic activity and photochromic state of nano-particulate silver surface loaded titanium dioxide thin-films. *Phys. Chem. Chem. Phys.* **2011**, *13*, 13827.

(15) Wang, M.; Al-Dhahir, I.; Appiah, J.; Koski, K. J. Deintercalation of zero-valent metals from two-dimensional layered chalcogenides. *Chem. Mater.* **2017**, *29*, 1650−1655.

(16) Kirczenow, G. Domain model of stage order and disorder in intercalation compounds. *Phys. Rev. B* **1985**, *31*, 5376−5386.

(17) Daumas, N.; Herold, A. Relations between phase concept and reaction mechanics in graphite insertion compounds. *C.R. Hebd. Seances Acad. Sci. Paris* **1969**, *268*, 373−375.

(18) Ratnaparkhe, A.; Kumar Radha, S.; Lambrecht, W. R. Calculated phonon modes, infrared and Raman spectra in orthorhombic α-MoO_3 and monolayer MoO_3. *J. Appl. Phys.* **2021**, *130*, 104302.

(19) Dresselhaus, M.; Dresselhaus, G. *Light scattering in solids III*; Springer, 1982; pp 3−57.

(20) Moulder, J. F.; Stickle, W. F.; Sobol, P. E.; Bomben, K. D.; Chastain, J. *Handbook of X-ray electron spectroscopy*; Physical Electronics Division, Perkin-Elmer Corp.: Eden Prairie, MN, 1992; pp 72−73.

(21) Fleisch, T.; Mains, G. An XPS study of the UV reduction and photochromism of MoO_3 and WO_3. *J. Chem. Phys.* **1982**, *76*, 780−786.

(22) Diaz-Droguett, D. E.; El Far, R.; Fuenzalida, V.; Cabrera, A. L. In situ-Raman studies on thermally induced structural changes of porous MoO_3 prepared in vapor phase under He and H2. *Mater. Chem. Phys.* **2012**, *134*, 631−638.